



Planetary Gearbox Fault Detection Using Vibration Separation Techniques

David G. Lewicki
Glenn Research Center, Cleveland, Ohio

Kelsen E. LaBerge
U.S. Army Research Laboratory, Glenn Research Center, Cleveland, Ohio

Ryan T. Ehinger
Bell Helicopter Textron Inc., Hurst, Texas

Jason Fetty
U.S. Army Aviation Applied Technology Directorate, Fort Eustis, Virginia

NASA STI Program . . . in Profile

Since its founding, NASA has been dedicated to the advancement of aeronautics and space science. The NASA Scientific and Technical Information (STI) program plays a key part in helping NASA maintain this important role.

The NASA STI Program operates under the auspices of the Agency Chief Information Officer. It collects, organizes, provides for archiving, and disseminates NASA's STI. The NASA STI program provides access to the NASA Aeronautics and Space Database and its public interface, the NASA Technical Reports Server, thus providing one of the largest collections of aeronautical and space science STI in the world. Results are published in both non-NASA channels and by NASA in the NASA STI Report Series, which includes the following report types:

- **TECHNICAL PUBLICATION.** Reports of completed research or a major significant phase of research that present the results of NASA programs and include extensive data or theoretical analysis. Includes compilations of significant scientific and technical data and information deemed to be of continuing reference value. NASA counterpart of peer-reviewed formal professional papers but has less stringent limitations on manuscript length and extent of graphic presentations.
- **TECHNICAL MEMORANDUM.** Scientific and technical findings that are preliminary or of specialized interest, e.g., quick release reports, working papers, and bibliographies that contain minimal annotation. Does not contain extensive analysis.
- **CONTRACTOR REPORT.** Scientific and technical findings by NASA-sponsored contractors and grantees.

- **CONFERENCE PUBLICATION.** Collected papers from scientific and technical conferences, symposia, seminars, or other meetings sponsored or cosponsored by NASA.
- **SPECIAL PUBLICATION.** Scientific, technical, or historical information from NASA programs, projects, and missions, often concerned with subjects having substantial public interest.
- **TECHNICAL TRANSLATION.** English-language translations of foreign scientific and technical material pertinent to NASA's mission.

Specialized services also include creating custom thesauri, building customized databases, organizing and publishing research results.

For more information about the NASA STI program, see the following:

- Access the NASA STI program home page at <http://www.sti.nasa.gov>
- E-mail your question via the Internet to help@sti.nasa.gov
- Fax your question to the NASA STI Help Desk at 443-757-5803
- Telephone the NASA STI Help Desk at 443-757-5802
- Write to:
NASA Center for AeroSpace Information (CASI)
7115 Standard Drive
Hanover, MD 21076-1320



Planetary Gearbox Fault Detection Using Vibration Separation Techniques

David G. Lewicki
Glenn Research Center, Cleveland, Ohio

Kelsen E. LaBerge
U.S. Army Research Laboratory, Glenn Research Center, Cleveland, Ohio

Ryan T. Ehinger
Bell Helicopter Textron Inc., Hurst, Texas

Jason Fetty
U.S. Army Aviation Applied Technology Directorate, Fort Eustis, Virginia

Prepared for the
67th Annual Forum and Technology Display (Forum 67)
sponsored by the American Helicopter Society (AHS)
Virginia Beach, Virginia, May 3–5, 2011

National Aeronautics and
Space Administration

Glenn Research Center
Cleveland, Ohio 44135

Level of Review: This material has been technically reviewed by technical management.

Available from

NASA Center for Aerospace Information
7115 Standard Drive
Hanover, MD 21076-1320

National Technical Information Service
5301 Shawnee Road
Alexandria, VA 22312

Available electronically at <http://www.sti.nasa.gov>

Planetary Gearbox Fault Detection Using Vibration Separation Techniques

David G. Lewicki
National Aeronautics and Space Administration
Glenn Research Center
Cleveland, Ohio 44135

Kelsen E. LaBerge
U.S. Army Research Laboratory
Glenn Research Center
Cleveland, Ohio 44135

Ryan T. Ehinger
Bell Helicopter Textron Inc.
Hurst, Texas 76053

Jason Fetty
U.S. Army Aviation Applied Technology Directorate
Fort Eustis, Virginia 23604

Abstract

Studies were performed to demonstrate the capability to detect planetary gear and bearing faults in helicopter main-rotor transmissions. The work supported the Operations Support and Sustainment (OSST) program with the U.S. Army Aviation Applied Technology Directorate (AATD) and Bell Helicopter Textron. Vibration data from the OH-58C planetary system were collected on a healthy transmission as well as with various seeded-fault components. Planetary fault detection algorithms were used with the collected data to evaluate fault detection effectiveness. Planet gear tooth cracks and spalls were detectable using the vibration separation techniques. Sun gear tooth cracks were not discernibly detectable from the vibration separation process. Sun gear tooth spall defects were detectable. Ring gear tooth cracks were only clearly detectable by accelerometers located near the crack location or directly across from the crack. Enveloping provided an effective method for planet bearing inner- and outer-race spalling fault detection.

Introduction

The U.S. Army has the goal of transitioning from traditional maintenance practices into Condition Based Maintenance (CBM) for its fleet of vehicles. Rotorcraft plays an important role in the Army fleet. The Army Aviation Applied Technology Directorate (AATD) and Bell Helicopter Textron teamed in a joint program titled Operations Support and Sustainment Technologies (OSST) (Ref. 1). The goal of this program was to mature and demonstrate new technology solutions to reduce the maintenance and support burden on current and future Army rotorcraft.

The drive systems of current rotorcraft play a significant role in overall safety and maintenance costs. In recent years, significant research has been devoted to the development of health and usage monitoring systems (HUMS) for drive systems (Refs. 2 to 6). Much of this activity has concentrated on gear and bearing fault detection. Planetary, or epicyclic, transmission configurations are used on many rotorcraft in the final stage of main-rotor drive systems. Planetary systems provide an efficient and compact method to reduce speed and have been used successfully for years in aerospace and automotive applications. Planetary systems, however, exhibit unique challenges relating to gear and bearing fault detection. First, multiple planets are contained in such systems. Since these planets all operate at the same speeds and loads, healthy components could potentially mask the vibration signatures of faulty components. Second, the planet gears exhibit epicyclic motion about a sun gear. Thus, the location of a faulty component, such as a planet tooth defect, changes position in time. This could provide a challenge for fixed-position accelerometers (usually mounted on the transmission housing) which measure the vibration signals that monitor component health. There has been some recent work in the development of planetary fault detection (Refs. 7 to 15), but most of these efforts were not validated for helicopter applications.

In support of the OSST activities, work was performed to mature planetary system fault detection methodologies. The objective of this work was to demonstrate the capability to detect planetary system gear and bearing faults in helicopter main-rotor transmissions. Experiments were performed on an OH-58C helicopter main-rotor transmission in the NASA Glenn 500-hp Helicopter Transmission Test Facility. A total of 15 tests were performed. The first test was with a healthy transmission. The next 12 tests used seeded-fault components simulating a cracked planet gear tooth, a spalled planet gear

tooth, a cracked sun gear tooth, a spalled sun gear tooth, a cracked ring gear tooth, and spalled planet bearings. The last two tests were blind demonstration tests in which the conditions of the transmission were unknown to the analyst. These consisted of a test with a simulated-cracked planet gear tooth and a test with all healthy components. Vibration data from the OH-58C transmission planetary system were collected and planetary fault detection algorithms were used to evaluate fault detection effectiveness.

Apparatus

Test Facility

The tests were performed in the NASA Glenn 500-hp helicopter transmission test facility (Fig. 1). The test stand operates on the closed-loop or torque-regenerative principle. Mechanical power re-circulates through a closed loop of gears and shafting, part of which is the test transmission. The output of the test transmission attaches to the bevel gearbox. The output shaft of the bevel gearbox passes through a hollow shaft in the closing-end gearbox and connects to the differential gearbox. The output of the differential attaches to the hollow shaft in the closing-end gearbox. The output of the closing-end gearbox attaches to the input of the test transmission, thereby closing the loop.

A 200-hp variable-speed direct-current (DC) motor powers the test stand and controls the speed. The motor output attaches to the closing-end gearbox, and functions to control speed and replenish losses due to friction in the loop. A 15-hp DC motor provides the torque in the closed loop and drives a magnetic particle clutch. The clutch output does not turn but exerts a torque. This torque is transferred through a speed-reducer gearbox and a chain drive to a large sprocket on the differential gearbox. The torque on the sprocket applies torque in the closed loop by displacing the gear attached to the output shaft of the bevel gearbox with respect to the gear connected to the input shaft of the closing-end gearbox. This is done within the differential gearbox through use of a compound planetary system where the planet carrier attaches to the sprocket housing. The magnitude of torque in the loop is adjusted by changing the electric field strength of the magnetic particle clutch.

A mast shaft loading system in the test stand simulates rotor loads imposed on the OH-58C transmission output mast shaft. The OH-58C transmission output mast shaft connects to a loading yoke. Two vertical load cylinders connected to the yoke produce lift loads. A single horizontal load cylinder connected to the yoke produces a bending load. A 2000-psig nitrogen gas system powers the cylinders. Pressure regulators connected to the nitrogen supply of each of the load cylinders adjust the magnitude of lift and bending.

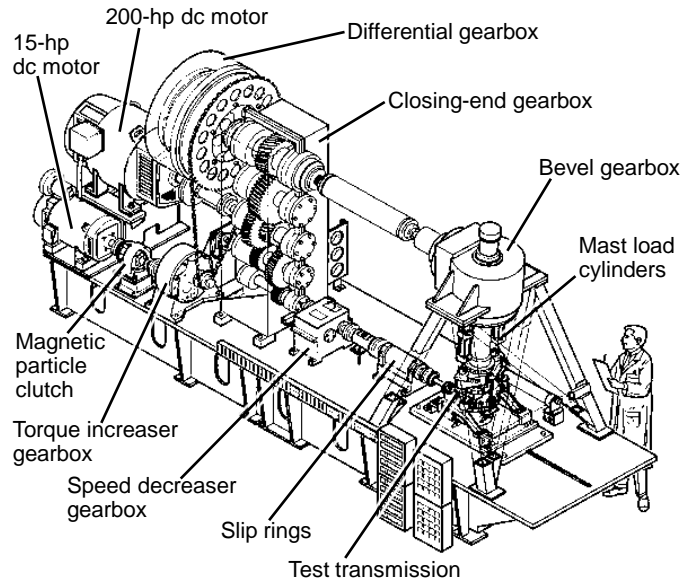


Fig. 1. NASA Glenn 500-hp helicopter transmission test facility.

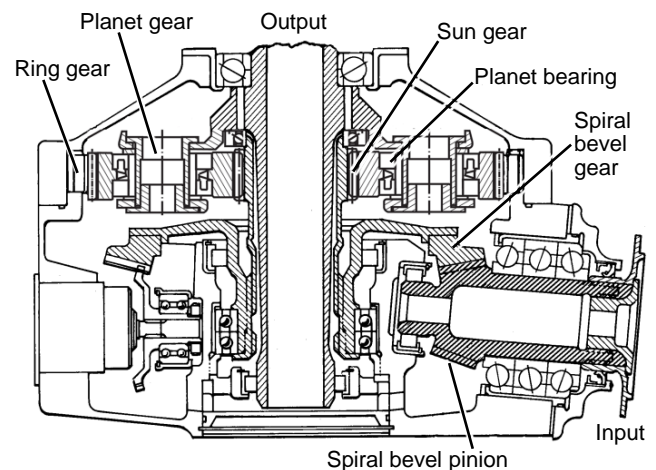


Fig. 2. OH-58C helicopter main-rotor transmission.

OH-58C Test Transmission

Tests were performed using an OH-58C helicopter main-rotor transmission (Fig. 2). The OH-58C transmission is rated at maximum continuous power of 335 hp at 6180 rpm input speed. The main-rotor transmission is a two-stage reduction gearbox with an overall reduction ratio of 17.44:1. The first stage is a spiral-bevel gear set with a 19-tooth pinion that meshes with a 71-tooth gear. Triplex ball bearings and one roller bearing support the bevel-pinion shaft. Duplex ball bearings and one roller bearing support the bevel-gear shaft.

The pinion is straddle mounted and the gear is overhung. A planetary mesh provides the second reduction stage. The bevel-gear shaft is connected through a spline to a sun gear shaft. The 27-tooth sun gear meshes with four 35-tooth planet gears, each supported with cylindrical roller bearings. The planet gears mesh with a 99-tooth fixed ring gear. The ring gear is connected to the transmission housing through a spline on its outer diameter. Power is taken out through the planet carrier which is connected to the output mast shaft through a spline. The output shaft is supported on top by a split-inner-race ball bearing and on the bottom by a roller bearing.

The OH-58C transmission is lubricated and cooled with its dedicated lubrication system. The 71-tooth bevel gear of the first reduction stage for the OH-58C transmission drives a 27-tooth accessory gear. The accessory gear runs an internal oil pump, which supplies pressurized oil. After passing through the standard OH-58C 10- μ m filter, the oil is ported to an external facility heater and heat exchanger, allowing precise control of oil inlet temperature. The oil is then routed back into the OH-58C transmission, providing lubrication for the gears and bearing through jets and passageways located in the transmission housing. The lubricant used in the OH-58C transmission was a synthetic base helicopter transmission oil conforming to the DOD-L-85734 specification. The nominal oil outlet pressure was 80 psig and regulated to 45 psig at the oil jets. The oil inlet temperature was 180 °F.

Test Components

A total of 15 tests were performed, as shown in Table I. Only healthy components were used for the baseline test (Test 1). All components for the baseline test were standard OH-58C production hardware except for the ring gear. The ring gear was modified to allow placement of a specially-designed fiber-optics strain sensors band (not described in this report), where portions of the ring gear outer-spline were removed to accommodate the band and cabling.

For Tests 2 and 3, one tooth of a planet gear was modified using the electrical discharge machining (EDM) method to simulate a cracked tooth (Table I). The crack/notch was placed in the tooth fillet region (where the largest tensile stress occurs) along the complete width of the tooth. The crack/notch had a crack depth of about 25 percent of the total tooth cross-section length and a circular path similar to that which would naturally occur (Ref. 16). Note that the planet gear is symmetric and can be installed “face-up” or “face-down” in the assembly. For Test 2, the planet was installed face-up so that the crack/notch tooth opened in tension when in mesh with the sun gear. Since the planet acts similar to an idler gear, the crack/notch tooth closed when in mesh with the ring gear. For Test 3, the planet was installed face-down so that the crack/notch tooth opened in tension when in mesh with the ring gear.

For Tests 4 and 5, one tooth of a planet gear was modified similar to that for Tests 2 and 3, but with a crack depth of about 50 percent of the total tooth cross-section length (Table I). For Tests 6 and 7, one tooth of a planet gear was modified using the EDM method to simulate a tooth spall defect (Table I). Here, an elliptical section of the meshing tooth surface was machined with a defect.

For Test 8, one tooth of a sun gear was modified using the EDM method to simulate a cracked tooth (Table I). The crack/notch was placed in the tooth fillet region along the complete width of the tooth and with a crack depth of about 25 percent of the total tooth cross-section length. For Test 9, a sun gear from a previous endurance test (Ref. 17) was used (Table I). The gear had a naturally generated tooth spall on one of its teeth.

For Tests 10 and 11, two additional ring gears were modified. One was modified to simulate a cracked tooth with a crack depth of about 25 percent of the total tooth cross-section length for Test 10, and the other was modified to simulate a cracked tooth with a crack depth of about 50 percent of the total tooth cross-section length for Test 11 (Table I). As with the healthy ring gear, both ring gears were modified to allow placement of the fiber-optics strain sensors band.

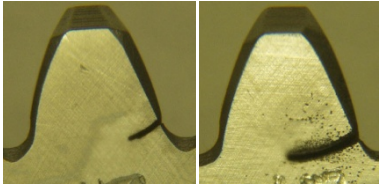
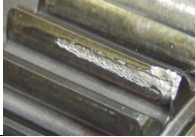
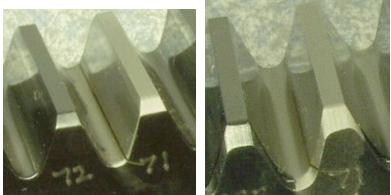
For Test 12, the outer race of a planet bearing was modified using the EDM method to simulate a bearing spall defect (Table I). The outer races of both rows of the two-row bearing were modified with a defect of about 0.10 in. length and 0.020 in. depth and along the complete race widths. For Test 13, the inner race of a planet bearing was modified using the EDM method to simulate a bearing spall defect (Table I). The inner race was modified with a defect of about 0.10 in. length and 0.020 in. depth and along the complete race width.

Test 14 was a blind repeat of Test 4. Here, one tooth of an additional planet gear was modified using the EDM method to simulate a cracked tooth with crack depth of about 50 percent of the total tooth cross-section length (Table I). Lastly, Test 15 was a blind repeat of the baseline Test 1 and consisted of all the same healthy components.

Instrumentation

Eight piezoelectric accelerometers were installed on the housing of the OH-58C transmission (Fig. 3). Six accelerometers (1, 2, 3, 4, 5, and 7) were directly mounted to the transmission housing adjacent to the ring gear through threaded holes. The holes were tapped in the housing at various positions along the circumference of the ring gear to measure vibration in the radial direction relative to the planetary. Two accelerometers (6 and 8) were mounted on brackets installed on the transmission top cover housing to measure vibration in the tangential direction relative to the planetary. For accelerometer 8, the bracket was mounted directly to the transmission housing. For accelerometer 6, the

TABLE I.—LIST OF TESTS PERFORMED.

Test	Description	Test component photo
1	Baseline test, all healthy components.	
2	Planet gear tooth crack, 25% depth, opened when in mesh with sun gear.	
3	Planet gear tooth crack, 25% depth, opened when in mesh with ring gear.	
4	Planet gear tooth crack, 50% depth, opened when in mesh with sun gear.	
5	Planet gear tooth crack, 50% depth, opened when in mesh with ring gear.	
6	Planet gear tooth spall at pitch line, in mesh with sun gear.	
7	Planet gear tooth spall at pitch line, in mesh with ring gear.	
8	Sun gear tooth crack, 25% depth.	
9	Sun gear tooth spall at pitch line.	
10	Ring gear tooth crack, 25% depth.	
11	Ring gear tooth crack, 50% depth.	
12	Planet bearing outer-race defect.	
13	Planet bearing inner-race defect.	
14	Demo test 1, Planet gear tooth crack, 50% depth, opened when in mesh with sun gear.	
15	Demo test 2, Baseline test, all healthy components.	

bracket was mounted on a top cover mounting stud. The accelerometers were commercially available and had a flat high-frequency response up to about 40 kHz and a resonant frequency of about 90 kHz. Coaxial fiber optic reflective scanners were mounted on both the OH-58C transmission input and output shafts to produce a once-per-rev tachometer pulse of each shaft. The OH-58 output shaft tachometer pulse was also routed to a facility data acquisition system totalizer and logic cards. The output of the logic card was programmed to produce a tachometer pulse for the planetary hunting tooth period of every 105 output shaft rotations of the OH-58C transmission.

The outputs of the accelerometers and tachometer pulses were routed to anti-aliasing filters and a PC-based data acquisition system. For all test cases and test conditions, data were acquired at 50 kHz sampling rate with a 25 kHz aliasing filter cut-off frequency. The data were acquired for 40 sec per set, with a total of ten sets for each test condition. The start of each data acquisition for each set was triggered by the planetary hunting tooth pulse. For the full operating speed of 6180 rpm OH-58 transmission input speed, the planetary hunting tooth period was 17.8 sec. Therefore, two complete and continuous planetary hunting tooth cycles were collected for each set and a total of 20 hunting tooth cycles were collected per test condition.

Assembly and Test Procedure

The planetary fault detection algorithms required precise knowledge as to which sun, planet, and ring gear teeth were in mesh at a given time. To do this, special indexing and a specific transmission assembly procedure were required.

The OH-58C planetary assembly is shown in Figure 4. First, the ring gear was positioned in the OH-58 transmission housing top cover so that a defined “tooth 1” was aligned with a fixed mark on the housing. Ring gear teeth were then numbered clockwise (as viewed from the bottom of the housing cover looking up, as in Fig. 4). Next, the OH-58 planets and sun gear were installed in the top cover housing. All tooth numbering was incremented in a clockwise manor. Tooth 1 of planet 1 was installed between teeth 1 and 2 of the ring gear, tooth 1 of planet 2 was installed between teeth 75 and 76 of the ring gear, and so on. Tooth 1 of the sun gear was positioned between teeth 18 and 19 of planet 1, tooth 22 of the sun gear was positioned between teeth 18 and 19 of planet 2, and so on. A special sun gear locking tool was then used to secure the planetary components. This kept the components from rotating, locking them in place, and allowed the complete assembly to flip for installation in the bottom case of the transmission. Once installed in the bottom case, the sun gear locking tool was removed without disturbing the planetary components and the transmission output shaft was installed. In this position, the output shaft tachometer was aligned so that the leading edge of the pulse was engaged. This procedure allowed precise position of the planetary tooth number indexing with respect to the transmission output tachometer and planetary hunting tooth tachometer.

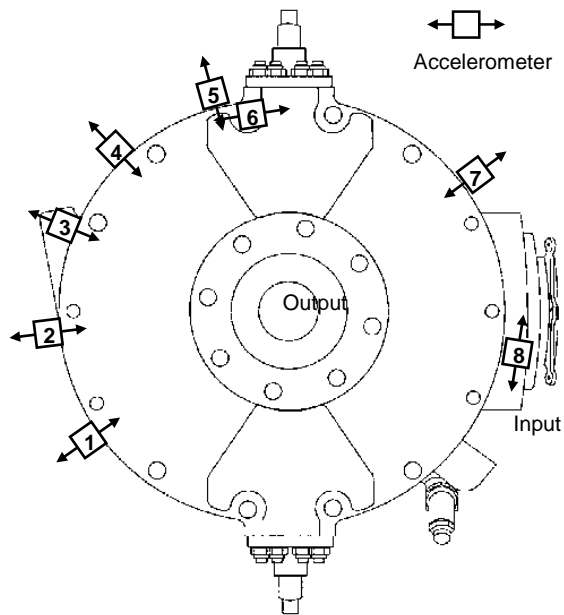


Fig. 3. Accelerometer locations on OH-58C transmission top cover housing, top view of cover housing.

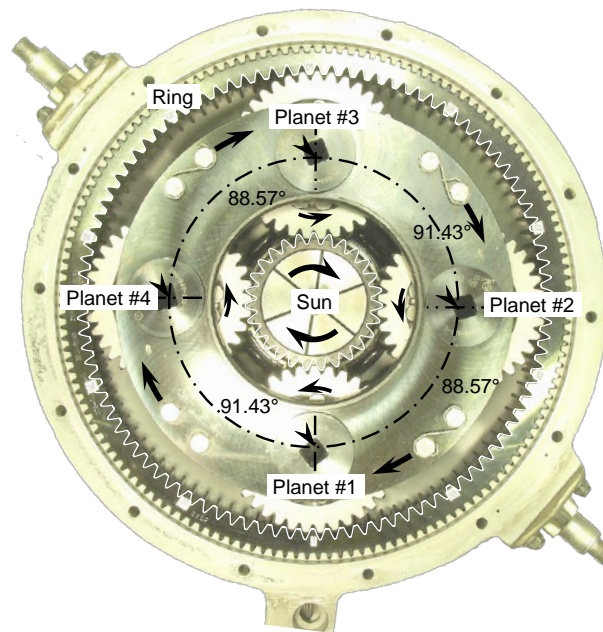


Fig. 4. OH-58C planetary assembly indexing definition at assembly, as viewed from the bottom of the housing cover looking up.

The test procedure for each of the 15 tests of Table I was the same. For each test, the OH-58C transmission was run at 16 different operating conditions consisting of four different torques (25, 50, 75, and 100 percent of design), two mast load conditions (full and off), and two speed conditions (6180 and 2060 rpm transmission input speed). For each test condition, the transmission was run until steady state was reached and then the vibration data were taken. As previously stated, 10 sets

of two complete and continuous planetary hunting tooth cycles were collected for a total of 20 hunting tooth cycles per test condition.

All data were digitized and recorded on a disk for later processing. At the end of each test, the transmission was stopped at the beginning of a hunting tooth cycle. The transmission was then removed from the facility and disassembled. The top cover housing containing the planetary was removed using the reverse of the previously described procedure. Again, the special locking tool was used to secure the planetary during disassembly. Using this disassembly procedure, the teeth positions for all planetary gears were oriented as in Figure 4 upon disassembly.

Fault Detection Methodology

Planet Bearing Fault Detection

Enveloping is a common method of detecting the health of stationary (non-orbiting) bearings. This method also proved to work well for detecting planet bearing faults, despite the orbiting planets. This method is well defined in Howard's review of rolling element bearing vibration (Ref. 18). The method is based on the knowledge that every time a rolling element passes by some raceway imperfection a short duration impulse excites bearing and structural natural frequencies. Enveloping analysis allows the extraction of the frequencies at which these impulses occur.

This particular project focused on inner- and outer-raceway defects. Equations for the inner-ball pass frequency and the outer-ball pass frequency are shown in Equations (1) and (2). These are the frequencies at which rolling elements pass an imperfection on the inner or outer race. Increases in the magnitude of the envelope spectrum at these frequencies are an indication of damage to the inner and outer races.

$$f_{b_{pfi}} = \frac{Z(f_o - f_i) \left(1 + \frac{d}{D} \cos \alpha\right)}{2} \quad (1)$$

$$f_{b_{pfo}} = \frac{Z(f_o - f_i) \left(1 - \frac{d}{D} \cos \alpha\right)}{2} \quad (2)$$

where $f_{b_{pfi}}$ is the inner-race defect frequency (Hz), $f_{b_{pfo}}$ is the outer-race defect frequency (Hz), Z is the number of balls or rollers, f_o is the bearing outer-race speed (Hz), f_i is the bearing inner-race speed (Hz), d is the ball or roller diameter (in.), D is the bearing pitch diameter (in.), and α is the contact angle ($^\circ$).

For the OH-58C planetary, $Z = 13$ rollers, $d = 0.4331$ in, $D = 2.264$ in, and $\alpha = 0^\circ$. At 100 percent input speed of 6180 rpm, the relative bearing speed is $(f_o - f_i) = 16.7$ Hz. Thus, the inner-race defect frequency is 129.4 Hz and the outer-race defect frequency is 87.8 Hz. Note that the faults induced in the

OH-58C planetary bearing were along both rows of the two row bearing. Since the rollers in the bearing rows are positioned offset from each other, the bearing acts like a 26-roller bearing instead of a 13-roller bearing. The pertinent inner- and outer-race defect frequencies were twice that of above, or 258.7 and 175.6 Hz, respectively.

A diagram for the calculation of the bearing condition indicators (CI's) is shown in Figure 5. The first 524,288 ($=2^{19}$) points of the raw data sampled at 50 kHz were used. The first step in enveloping was to run the raw data through a band pass filter with a pass band around structural frequencies, usually between 20 and 40 kHz. Through trial and error, a high-pass filter with a cutoff frequency of 18 kHz was found to work well for this application, giving usable band pass data from 18 to 25 kHz. After filtering, a Hilbert transform was computed. The Hilbert transform, $H(n)$, is effectively a 90° phase shift in the time domain. The Hilbert transform data, $H(n)$, and the filtered data, $A(n)$, were combined into what is known as the analytic signal, $A'(n)$, defined as follows:

$$A'(n) = A(n) + iH(n) \quad (3)$$

The magnitude of this analytic signal gives the envelope signal. The health of the bearing raceways can be determined by examining the values of vibration at the bearing inner- and outer-race defects from the frequency spectrum of this analytic signal.

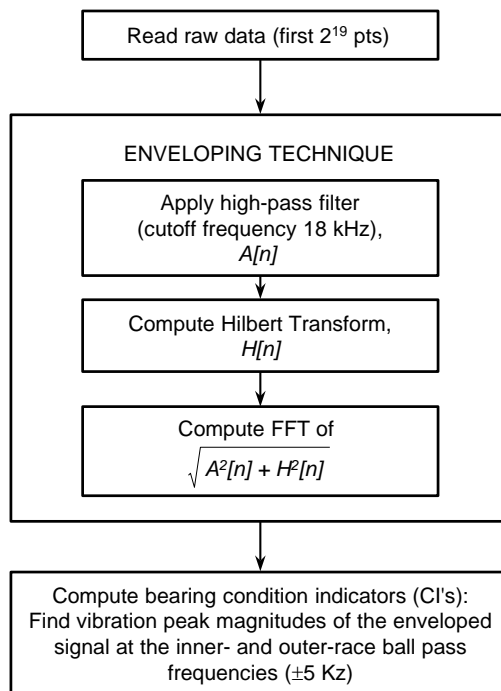


Fig. 5. Bearing fault detection technique.

Planet Gear Fault Detection

A flowchart of the planet gear fault detection methodology is shown in Figure 6. The methodology used was a modified version of McFadden’s method of separating planet vibrations (Refs. 8, 10, and 12). The first step was to take the raw data and separate it into hunting tooth cycles. The hunting tooth cycles were then re-sampled (using linear interpolation) with respect to each carrier cycle, so that every carrier cycle contained the same number of points. This accounted for any speed variations within the hunting tooth cycle. The number of points in each carrier cycle were set to be an integer multiple of the number of ring gear teeth. A total of 8415 points (99 ring gear teeth x 85 points per tooth) were used for each carrier cycle. This was the greatest number of ring gear multiples that was still less than the original number of points from the raw data. For each test condition, data from 20 hunting tooth cycles for a given accelerometer were averaged together using this procedure to produce one average hunting tooth cycle, which will hereon be defined as a hunting tooth average (HTA). As previously stated, a hunting cycle was 105 carrier cycles, or 17.8 sec in duration for tests at 6180 rpm input speed. This procedure was repeated for each accelerometer.

The next step was to separate out the data for each planet into tooth vectors. Separation involved grabbing sections of data as each planet passed a particular accelerometer, multiplying it by some windowing function and then adding it into a tooth vector for that planet according to the planet tooth that was in mesh at the sensor location. The planet positions at the output tachometer pulse and the sequence of the teeth that mesh with each sensor were known beforehand. At the start of a given test, the initial planet positions were known from the planet assembly procedure (Fig. 4). The sequence of teeth in mesh were determined from the number of teeth on the ring gear and planet gears (Ref. 12). For the OH-58C application, all planet teeth pass by a particular sensor position due to the hunting tooth relationship between the planets (35 teeth) and ring gear (99 teeth). A window with tapered edges was selected that satisfied the criteria set forth in (Ref. 10). A Tukey window was chosen for this application. A Tukey window is similar to a raised cosine (Hanning) window, with a hold at a gain of one in the middle. After evaluating several window width designs, a Tukey window of five-teeth wide with a hold for one tooth in the center was chosen.

Every time a planet passed an accelerometer, a five-tooth wide section of data was sectioned and multiplied by the

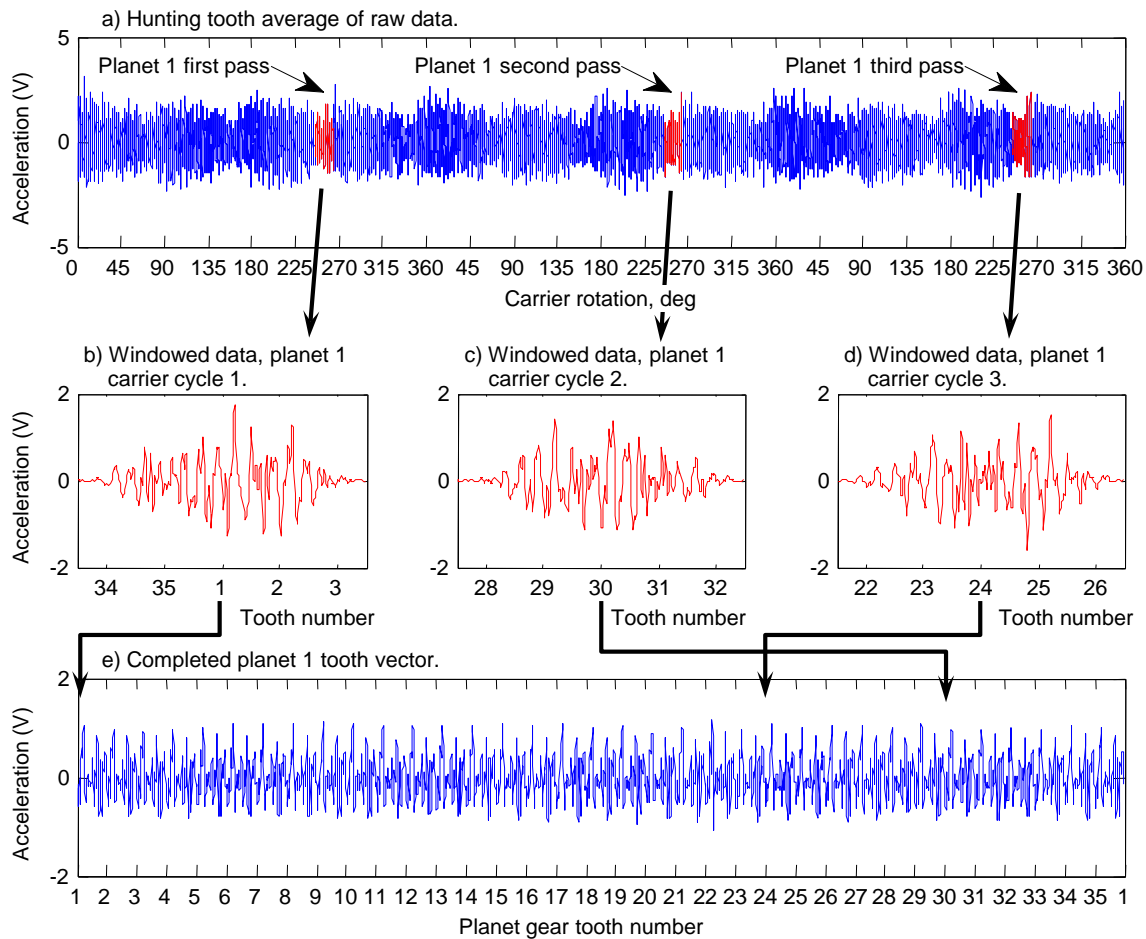


Fig. 6. Planet gear tooth vibration separation fault detection technique.

selected Tukey window. The window was then added into a tooth vector according to planet centered on the tooth in mesh at that point (Fig. 6). Once the windows were assembled, the values of the tooth vectors were divided by a factor of 9. This was due to a window gain factor of 3 for a Tukey window of five-teeth wide and a hold for one tooth, and a factor of 3 due to three planet cycles in a hunting tooth cycle. Each planet vector had 2975 number of points (35 planet teeth x 85 points per tooth). Each planet vector was then resampled down to 2048 points (even power of two) for ease in Fourier Transform calculations. This process was performed for all planets and all accelerometers. Thus, for each test condition, 32 planet vectors (4 planets x 8 accelerometer) were assembled. Condition indicators (CI's) were then applied to each planet vector.

Sun Gear Fault Detection

The separation of time averages for the sun gear was slightly more complicated. Sun teeth are only “seen” by accelerometers through the passing planets where the accelerometers are mounted on the housing near the ring gear. McFadden presents his method as applicable for both sun and planet gears. However, the sun gear brings up a different set of complications. If sun teeth are only viewed through the passing planets, all sun teeth aren't necessarily seen. In the OH-58C main transmission application, three sun gear teeth are viewed by an accelerometer for a particular planet due to the non-hunting tooth virtual relationship between the sun gear (27 teeth) and ring gear (99 teeth). The same three teeth are also viewed by the accelerometer for the planet directly opposite (180° apart). Three additional sun teeth are viewed by the accelerometer for the remaining two planets. Thus, for the OH-58C, only six of the sun teeth are viewed by a particular accelerometer through the passing planets. In addition, these teeth are not evenly spaced around the sun. The OH-58C has neighboring planets that are either 91.4° or 88.6° apart, with even or odd planets 180° apart (see Fig. 4). This results in uneven spacing of the sun teeth viewed since the planet are not evenly spaced at 90° to each other.

There are two ways to deal with these issues. The first option is to average the data from all the passing planets into a single sun tooth vector. While this method allows the smallest window to be used, the windows must be asymmetric in order to account for uneven spacing between the teeth viewed. This also involves averaging data from different planets together, each of which have their own vibration signature. The second option is to generate four separate sun gear tooth vectors per accelerometer, each one being the sun vibration as seen through an individual planet. This method requires a wider window because only three sun teeth are viewed through each planet. These teeth, however, are evenly spaced around the sun since a given sun vector is seen through only one given planet. Several iterations of each option were tried, but the best results were obtained using the second option with a symmetric Tukey window that was 27-teeth wide with a hold of one for nine teeth in the center.

Ring Gear Fault Detection

The method used to obtain time averages of the ring gear was fairly simple. Taking the hunting tooth average, each carrier cycle was averaged. This data set was used as the ring gear tooth vector. One set of ring data then included the data of all four passing planets. Therefore, ring gear damage would be seen four times in the ring time average because it is loaded four times by the passing planets.

Condition Indicators

A total of nine condition indicators (CI's) were used to determine the health of the gears in the planetary system. All of these indicators were previously developed for single gear sets and were applied to the separated sun, planet, and ring gear tooth vectors discussed above. Indicators were also calculated directly from the hunting tooth average (HTA). This was done to gauge the benefit of performing the extra vibration separation processing. In calculating the indicators for the HTA, only the first 2^{18} points were used because it was found that using the full HTA was time intensive and the results obtained using fewer points were nearly identical.

Before computing the CI's, the bevel meshing frequency was removed from the sun, ring, and HTA signals. The assembly of planet tooth vectors was such that the bevel meshing frequency was averaged out with no further processing needed.

The nine CI's used were RMS, crest factor, energy ratio, FM0, kurtosis, energy operator, FM4, M6A and M8A. All of these indicators are explained in (Ref. 19). Condition indicator M8A performed the best in this study and will be the only one discussed in this report. The parameter M8A, proposed by Martin (Ref. 20), uses the eighth moment normalized by the variance to the fourth power and is given as

$$M8A = \frac{N^3 \sum_{i=1}^N (\delta_i - \bar{\delta})^8}{\left[\sum_{i=1}^N (\delta_i - \bar{\delta})^2 \right]^4} \quad (4)$$

where N is the number of samples, i is the sample index, δ is the difference signal, and $\bar{\delta}$ is the mean of the difference signal. The difference signal, δ , is defined as

$$\delta = x(t) - y_d(t) \quad (5)$$

where $x(t)$ is the original time synchronous signal and $y_d(t)$ is the signal containing the component shaft frequency, the gear mesh frequency, their harmonics, and their first-order sidebands. For this project, the best results were obtained by only removing the fundamental gear meshing frequency and the first ten harmonics. For planet and sun gears, the stop-band width used was three shaft orders. Ring gears were more complicated because the planets pass four times within the gear rotation. The difference signal was most sensitive to damage when a stop-band width of 16 times the output frequency was

removed. The stop-band for the HTA data also included the planet pass envelope. From previous work, it was found that the first-order sidebands occur at a sideband width equal to the planet pass frequency. Therefore, the stop-band width used in calculating the HTA difference signal was slightly more than eight times the carrier frequency.

Results and Discussion

Planet Gear Tooth Defects

Test 2 used a planet gear with an EDM-simulated tooth crack, 25 percent depth, in planet 1, tooth 17, installed face up such that the crack opened when in mesh with the sun gear. Test 3 used the same cracked planet gear as Test 2, but installed face down such that the crack opened when in mesh with the ring gear. By definition, tooth 1 on the planet gear was the same physical tooth for Tests 2 and 3. For both tests, the planet teeth numbering on the gear faces was incremented in a counter clockwise direction as viewed from the bottom of the housing cover looking up. Thus, the cracked tooth was defined as tooth 17 for Test 2 and tooth 20 for Test 3. Test 4 and 5 were similar to Test 2 and 3, respectively, but used a planet gear with a simulated tooth crack of 50 percent depth.

Figure 7 shows the effect of a crack on planet 1 tooth vectors and difference signals for accelerometer 1 at 100 percent torque, speed, and mast loads. The planet gear tooth vectors and difference signals for Tests 1 and 4 are plotted against planet gear tooth number, which is defined as the planet tooth number in mesh with the ring gear at the location of the accelerometer. Figures 7a and 7c are for the baseline Test 1 of all healthy components. Repeated vibration patterns for each tooth for both the planet gear tooth vector and difference signal plots are evident. By comparison, Figure 7b and 7d are for Test 4 with a planet gear tooth crack of 50 percent depth. At planet gear tooth number 17 in Figure 7, the crack was closed and in mesh with the ring gear. At tooth number 35, the crack was opened and in mesh with the sun gear. The effect of the crack was clearly seen in Figure 7d as a disturbance in the difference signal at tooth 18 and at tooth 1 (or end of tooth 35 since the plot is periodic). The crack was more detectable when forced closed at the ring rather than when opened at the sun. It was believed that the crack closing behavior was more discernable because the planet cracks were machined notches with a gap at the crack region. Without this removal of material, the dominant crack closing behavior at tooth 18 is expected to be greatly reduced if not eliminated. This would probably reduce the fault detection effectiveness of a CI, but how much is not presently known. Note that planet faults were seen in tooth vectors one tooth after going through mesh with the ring. This is probably due to backlash and windup of the complete system (OH-58C test transmission and facility gearboxes) under torque.

Figure 8 shows the effect of a planet tooth crack on M8A for all accelerometers at 100 percent speed, torque, and mast loads for Tests 1 and 4. Again, M8A responds to the spikiness of a signal, so that disturbances in the difference signal, such as in

Figure 7d, can be identified. From Figure 8, strong indications of a defect are given for accelerometers 1, 2, 3, and 8, while small to moderate indications are given for accelerometers 4, 5, 6, and 7.

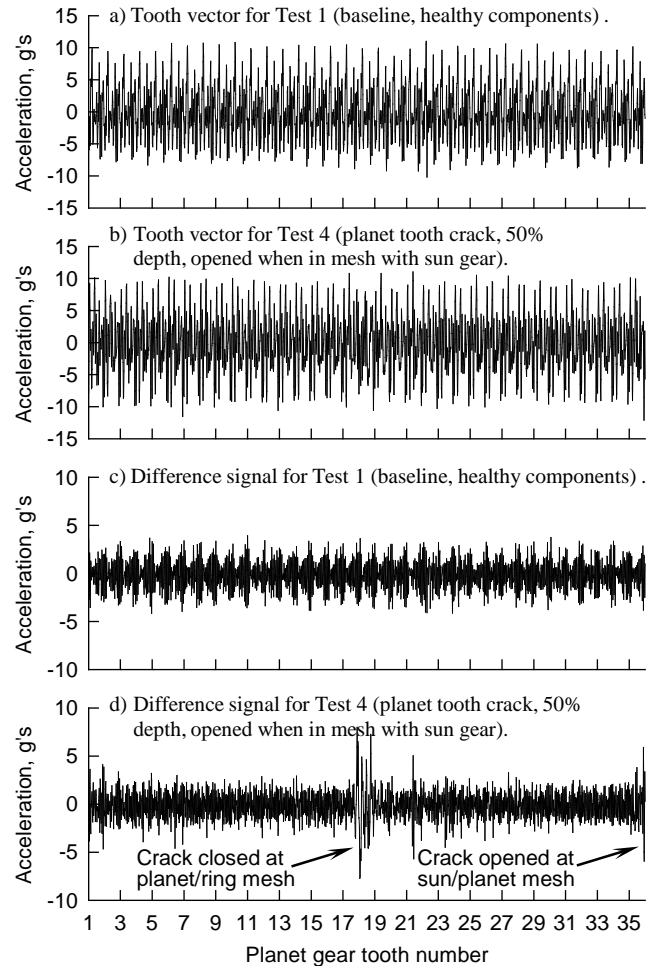


Fig. 7. Effect of crack on planet 1 tooth vectors and difference signals, for accelerometer 1 at 100% speed, torque, and mast loads.

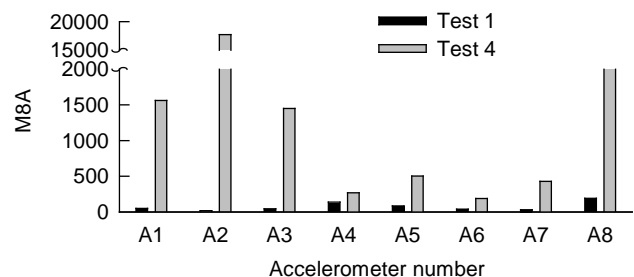


Fig. 8. Effect of crack on planet 1 M8A for all accelerometers, at 100% speed, torque, and mast loads. Test 1: baseline, healthy components; Test 4: planet tooth crack, 50% depth, opened when in mesh with sun gear.

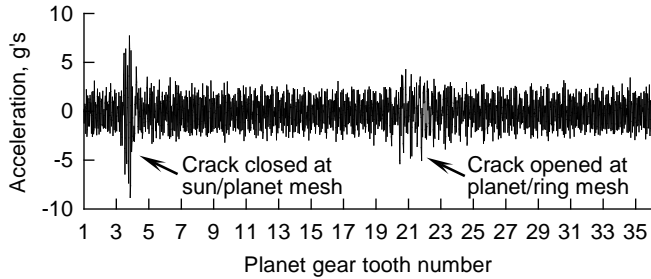


Fig. 9. Planet 1 difference signal for Test 5 (planet tooth crack, 50% depth, opened when in mesh with ring gear), for accelerometer 1 at 100% speed, torque, and mast loads.

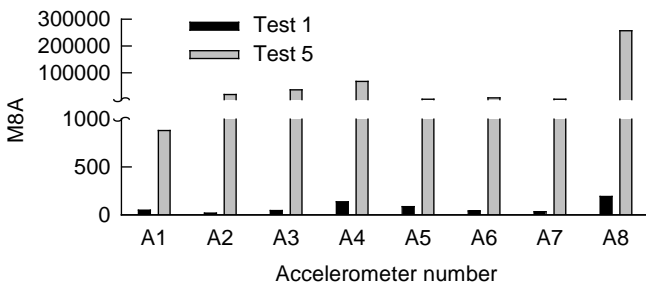


Fig. 10. Effect of crack on planet 1 M8A for all accelerometers, at 100% speed, torque, and mast loads. Test 1: baseline, healthy components; Test 5: planet tooth crack, 50% depth, opened when in mesh with ring gear.

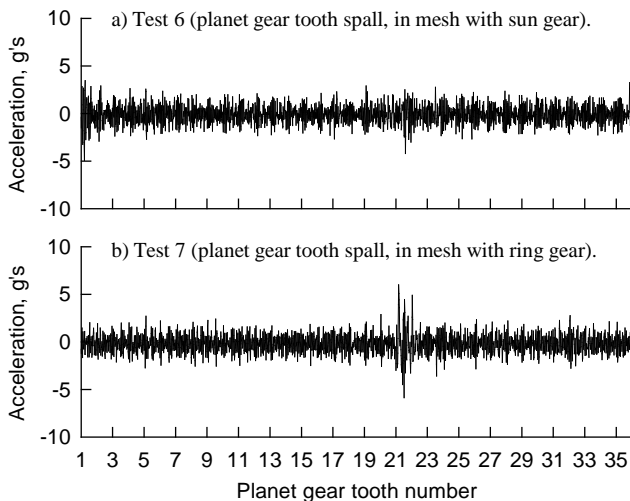


Fig. 11. Effect of meshing gear on planet 1 difference signals for planet gear tooth spall tests, for accelerometer 1 at 100% speed, torque, and mast loads.

Figure 9 shows the effect of a crack on the planet 1 difference signal for Test 5 for accelerometer 1 and at 100 percent torque, speed, and mast loads. Here, a strong disturbance is seen at tooth 4 due to the crack being closed at the sun-planet mesh. Also, a disturbance is seen at tooth 21 for the planet-ring mesh (crack being opened). Figure 10 gives the M8A results for all accelerometers of Test 5. All accelerometers give a strong indication of the defect as compared to the baseline test. Figures 7 through 10 show the fault detectability for the crack with 50 percent depth. Similar results for the 25 percent depth crack tests were seen although not as pronounced.

It was observed from many of the seeded-fault tests that the vibration irregularities that occurred during the passing of a fault through the sun-planet mesh bled through to all the planets. This was observed from the difference signals of the planet 1 through 4 tooth vectors and resulting M8A indications. This was thought to be a result of the sun gear, which has a floating center, to displace slightly and affect the meshing action of all the planets during passing of a defect. Due to the bleed through, it may be difficult, in some cases, to distinguish a fault to a particular individual planet. This, however, should not be an issue in actual helicopter applications since it would be more than adequate to identify a faulty planetary system and not an individual planet gear.

Figure 11 shows the effect of planet gear tooth spalling on the difference signals for planet 1 of Tests 6 and 7, accelerometer_1, and at 100 percent torque, speed, and mast loads. The spall was an EDM-machined defect, elliptical in shape, approximately 0.020-in. in depth, and centered along the gear tooth face width and the pitch line. The spall was placed on tooth 17 for Test 6 (planet tooth spall in mesh with the sun gear), and also defined as tooth 20 for Test 7 (planet tooth spall in mesh with the ring gear). For Figure 11a, the defect is faintly seen at planet tooth number 1 (planet-ring mesh), which is diametrically opposite tooth 17 (sun-planet mesh). For Figure 11b, the defect is very noticeable at planet tooth 21. The effect of planet gear spalling on M8A is shown in Figure 12 for all accelerometers at 100 percent speed, torque, and mast loads. Many of the accelerometers gave an indication of the defect. As with the planet gear tooth crack test, some leakage of the defect signals to the neighboring planets occurred when the planet fault went through mesh at the sun gear.

Lastly, it should be noted that the planet tooth defects were not clearly distinguishable in the HTA signals. Thus, the planet gear tooth separation technique described in this study provided an effective means to detect planet tooth defects.

Sun Gear Tooth Defects

Test 8 used a sun gear with an EDM-simulated tooth crack, 25 percent depth, on tooth 8, oriented such that the crack opened when in mesh with the planet gears. Test 9 used a sun

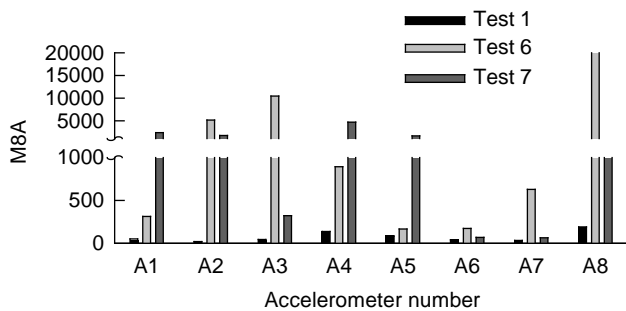


Fig. 12. Effect of spall and meshing gear on planet 1 M8A for all accelerometers, at 100% speed, torque, and mast loads. Test 1: baseline, healthy components; Test 6: Planet gear tooth spall at pitch line, in mesh with sun gear; Test 7: Planet gear tooth spall at pitch line, in mesh with ring gear.

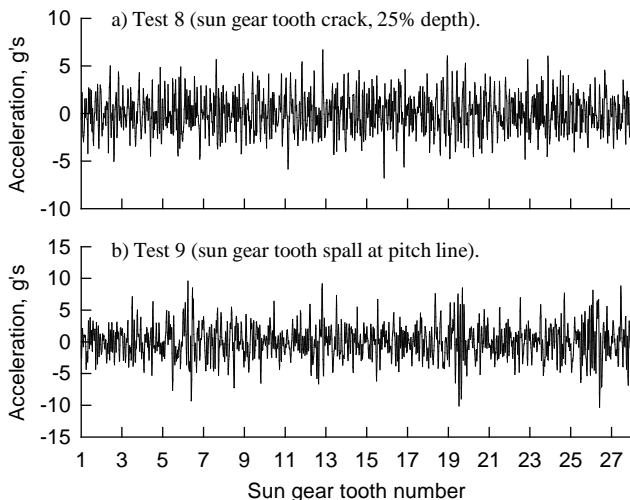


Fig. 13. Difference signals from sun gear tooth fault tests, for sun-to-planet 1 transfer path for accelerometer 1 at 100% speed, torque, and mast loads.

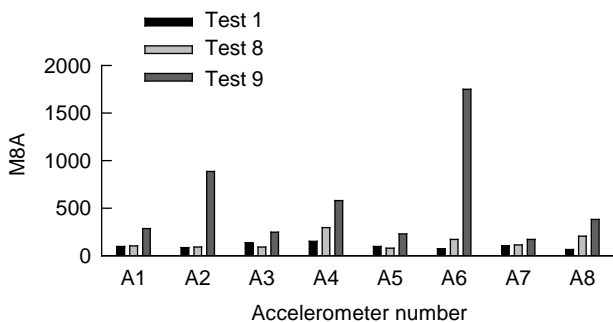


Fig. 14. Effect of sun gear tooth faults on M8A, for sun-to-planet 1 transfer path, at 100% speed, torque, and mast loads. Test 1: baseline, healthy components; Test 8: sun gear tooth crack, 25% depth; Test 9: sun gear tooth spall at pitch line.

gear with a natural occurring spall defined on tooth 8, also oriented such that the spall was in mesh with the planet gears. Figure 13 gives the difference signals for accelerometer 1 of Tests 8 and 9 at 100 percent speed, torque, and mast loads. Figure 14 gives the M8A results.

The horizontal axis of Figure 13 is defined as the sun gear tooth number in mesh with planet 1 at the location of accelerometer 1. This, however, is fundamentally different than that for the planet gear analysis (Figs. 7, 9, and 11). For the planet gear analysis, every tooth of a planet gear was in mesh with the ring gear at a given location of an accelerometer due to the hunting tooth meshing action. Thus, the planet tooth vectors are made up of 35 distinct regions summed together with centers at each tooth number. For the sun analysis of the OH-58C, only three sun gear teeth were in mesh with a given planet at a given accelerometer position. Figure 13, as an example, is made up of three distinct regions summed together with centers at sun gear tooth 3, 12, and 21 for accelerometer 1 and planet 1. Thus, the sun gear results are less sensitized than the planet gears with respect to analysis of individual teeth. This made the sun gear tooth crack defect difficult to detect (Fig. 13a). Also, the difficulty to detect the sun gear tooth crack (as indicated by M8A in Fig. 14) was noticed for all accelerometers.

The sun gear spall defect was detectable, but not as apparent as the planet gear faults. A slight disturbance at tooth 7 in Figure 13b is seen (spalled sun in mesh with planet). Three more disturbances can be seen in the figure to correlate when the other planets were in mesh with the spalled sun tooth. This was due to the leakage effect as described in the planet defect section. Accelerometers 2 and 6 gave an indication of the sun tooth spall as indicated by M8A in Figure 14. It is not clear at this time as to why these accelerometers performed better than the others. The ability to detect the spall did not appear to correlate to when the spalled sun gear tooth was in direct alignment (through a planet) with an accelerometer.

Ring Gear Tooth Defects

Test 10 was run with a simulated ring gear tooth crack, 25 percent in depth, on ring gear tooth 71, which was aligned with accelerometer 1. Test 11 was similar, but with a 50 percent depth crack. Figure 15 gives the ring gear difference signals for accelerometer 1 at two different torque conditions, 50 and 100 percent. The horizontal axis is defined as the ring gear tooth number in contact with planet 1. The data of the figure is time-averaged and the period is one-carrier rotation. Due to the four passing planets within the carrier cycle, the fault was seen four times in the accelerometer 1 tooth vector. This was seen when planet 1 was in mesh with ring teeth 22 (planet 3 pass), 46 (planet 4 pass), 71 (planet 1 pass), and 96 (planet 2 pass). The fault is more evident for the 50 percent torque test conditions than the 100 percent torque condition.

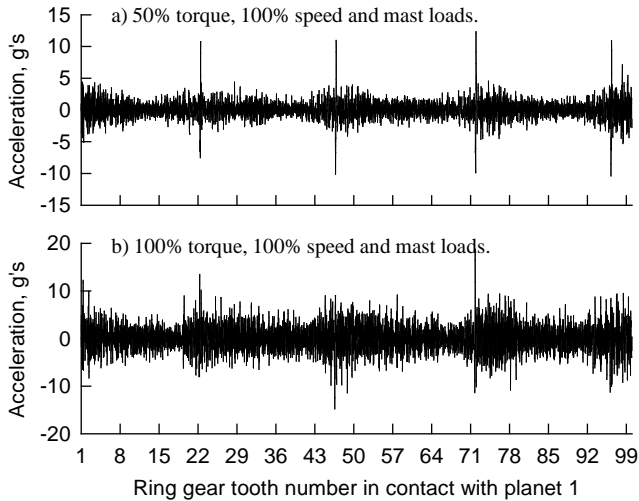


Fig. 15. Effect of torque on difference signals for Test 11 (ring gear tooth crack, 50% depth), for accelerometer 1.

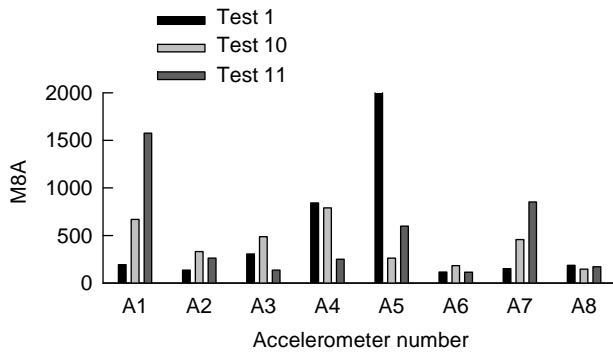


Fig. 16. Effect of ring gear tooth defect on M8A for all accelerometers, at 100% speed, torque, and mast loads. Test 1: baseline, healthy components; Test 10: ring gear tooth crack, 25% depth; Test 11: ring gear tooth crack, 50% depth.

For the other accelerometers, the ring gear crack was difficult to detect. Figure 16 gives the M8A results for all accelerometers at 100 percent speed, torque, and mast loads. As seen in the figure, accelerometer 1 shows the most detectability of the defect. For accelerometers not aligned with a cracked ring gear tooth, fault detection was difficult. The only exception was accelerometer 7. This accelerometer gave a moderate indication of the defect. Accelerometer 7 was positioned 180° opposite accelerometer 1, and thus in direct contact with the defect through the ring, planets, and sun gears.

Planet Bearing Defects

Test 12 was run with a localized defect on the outer race of planet 1 that extended across both rows of the bearing race. Test 13 was performed with a localized defect on the inner race of the planet 1 bearing that extended across both rows of the bearing race. Figure 17 shows the results from the enveloping technique for fault detection for the seeded-fault bearing tests.

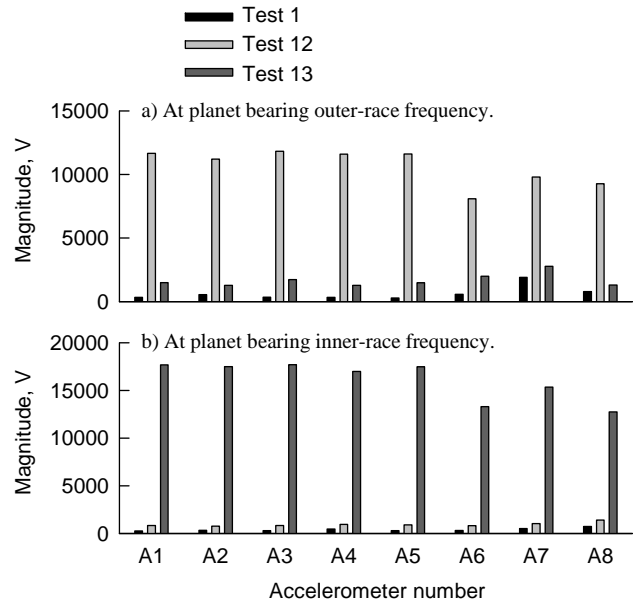


Fig. 17. Enveloped spectrum vibration at bearing race frequencies for all accelerometers, at 100% speed, torque, and mast loads. Test 1: baseline, healthy components; Test 12: planet bearing outer-race defect; Test 13: planet bearing inner-race defect.

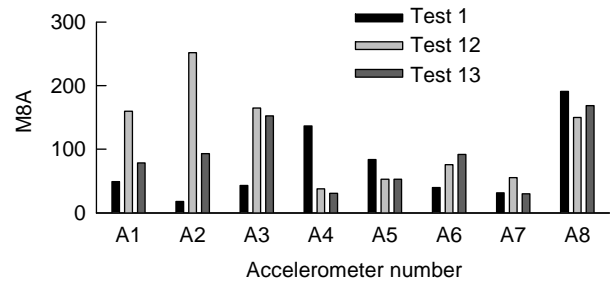


Fig. 18. Effect of planet bearing defect on M8A (relative to planet 1 gear tooth fault) for all accelerometers, at 100% speed, torque, and mast loads. Test 1: baseline, healthy components; Test 12: planet bearing outer-race defect; Test 13: planet bearing inner-race defect.

Figure 17a gives the vibration magnitude at the outer-race frequency, previously calculated as 175.6 Hz. A clear and distinct increase in vibration of the outer-race frequency is depicted for the planet bearing outer-race defect test (Test 12). Figure 17b gives the vibration magnitude at the inner-race frequency, previously calculated as 258.7 Hz. A clear and distinct increase in vibration of the inner-race frequency is depicted for the planet bearing inner-race defect test (Test 13). Therefore, for these tests, the enveloping technique provided an effective way to detect bearing race defects.

Figure 18 gives the results of the planet gear fault analysis for the data from the planet bearing fault tests. Shown is the M8A results of the planet tooth 1 vector difference signal, for all accelerometers at 100 percent, torque, and mast loads. No

apparent trend is observed, which implies that the planet bearing fault does not give rise to a faulty indication of a planet gear tooth fault.

Blind Tests

In an effort to demonstrate the diagnostic capabilities developed, two blind demonstration tests were run. During these demonstration tests, the researcher processing the data had no prior knowledge as to the health of the transmission. It was established beforehand that the faults used in demonstration tests were to be limited to those previously run in seeded-fault Tests 1 through 13.

A fault detection procedure was developed prior to processing demonstration test results. This procedure used an “expert system” type methodology, where trends for each seeded-fault test were assembled and rules based on CI exceedance were compiled. The primary contribution for gear tooth fault detection was the M8A condition indicator based on the planet, sun, and ring gear tooth vectors. This was collected for all accelerometers and run conditions from each test. In addition, the vibration levels of the bearing race frequencies from the enveloped spectrums were used for bearing fault detection. Unique rules and thresholds for fault detection of each test case were developed.

Tests 14 and 15 were the two blind tests which were performed and analyzed using this methodology to predict which gearbox components were faulty. Test 14 used a planet gear with an EDM-simulated tooth crack, 50 percent depth, in planet 3, tooth 9, installed face up such that the crack opened when in mesh with the sun gear. This defect was correctly detected from the strong indications in the planet 3 tooth vectors and corresponding M8A results. Test 15 was the second blind test and consisted of the same all healthy components as the baseline Test 1. Unfortunately, a ring gear tooth crack defect was predicted from the analysis rather than a healthy transmission. The results were not distinctly indicative of a ring gear fault, but varied slightly enough from the baseline to give an erroneous false alarm prediction.

Conclusions

Studies were performed to demonstrate the capability to detect planetary gear and bearing faults in helicopter main-rotor transmissions. The work supported the Operations Support and Sustainment Technologies (OSST) program with the U.S. Army Aviation Applied Technology Directorate (AATD) and Bell Helicopter Textron. To support the OSST goal of maturing technology to reduce maintenance costs, experiments were performed on an OH-58C helicopter main-rotor transmission in the NASA Glenn 500-hp Helicopter Transmission Test Facility. Vibration data from the OH-58C planetary system were collected on a healthy transmission as well as with various seeded-fault components. Planetary fault detection algorithms were used with the collected data to evaluate fault

detection effectiveness. A total of 15 tests were performed in the project. These consisted of tests on a healthy transmission and tests on different seeded-fault components such as planet tooth cracking, planet tooth spalling, sun tooth cracking, sun tooth spalling, ring tooth cracking, planet bearing spalling, and two blind demonstration tests. The following conclusion were derived:

1. Planet gear tooth cracks and spalls were detectable using the vibration separation techniques described in the paper.
2. Vibration during passing of a planet gear tooth defect bled through to other planets through the sun gear movement and was discernable by observation of the condition indicators from all planet tooth vectors.
3. A greater change in vibration was noticed when a machined crack was being closed during mesh rather than being opened during mesh. This was probably caused by the finite width of the machined crack/notch defect.
4. Sun gear tooth root cracks were not discernibly detectable from the vibration separation process.
5. Sun gear tooth spall defects were detectable.
6. Ring gear tooth cracks were only clearly detectable by accelerometers located near the crack location or directly across from the crack.
7. Enveloping provided an effective method for planet bearing inner- and outer-race spalling fault detection.
8. A planet tooth crack was correctly identified for the first blind demonstration test. Some scattered results for the second blind demonstration test prevented the correct identification of a healthy transmission.

References

1. Baker, T., Augustin, M., Ferrie, C., Thompson, B., and Yeary, D., “Operations Support and Sustainment Technologies for Current and Future Aircraft,” Proceedings of the American Helicopter Society 65th Annual Forum, Grapevine, TX, May 26–29, 2009.
2. Grabill, P., Brotherton, T., Berry, J., and Grant, L., “The U.S. Army and National Guard Vibration Management Enhancement Program (VMEP): Data Analysis and Statistical,” Proceedings of American Helicopter Society 58th Annual Forum, Montreal, Quebec, Canada, June 11–13, 2002.
3. Dousis, D., and Strohmeyer, M., “V-22 Mechanical Systems Vibration Monitoring Field Operations Experience,” Proceedings of American Helicopter Society 63rd Annual Forum, Virginia Beach, VA, May 1-3, 2007.
4. Bechhoefer, E., Duke, A., and Mayhew, E., “A Case for Health Indicators vs. Condition Indicators in Mechanical Diagnostics,” Proceedings of American Helicopter Society 63rd Annual Forum, Virginia Beach, VA, May 1–3, 2007.
5. Keller, J., Carr, D., Love, F., Grabill, P., Ngo, H., and Shanthakumaran, P., “AH-64D Main Transmission Accessory Drive Spur Gear Installation Fault Detections,” Proceedings of the American Helicopter Society Technical Specialists' Meeting on Condition Based Maintenance, Huntsville, AL, Feb. 10–11, 2009.
6. Antolick, L., Branning, J., Dempsey, P., and Wade, D., “Evaluation of Gear Condition Indicator Performance on

- Rotorcraft Fleet,” Proceedings of the American Helicopter Society 66th Annual Forum, Phoenix, AZ, May 11–13, 2010.
7. McFadden, P.D., and Smith, J.D., “An Explanation for the Asymmetry of the Modulation Sidebands About the Tooth Meshing Frequency in Epicyclic Gear Vibration,” Proceedings of the Institution of Mechanical Engineers, Part C, Journal of Mechanical Engineering Science, Vol. 199, pp. 65–70, 1985.
 8. McFadden, P.D., “A Technique for Calculating the Time Domain Averages of the Vibration of the Individual Planet Gears and the Sun Gear in an Epicyclic Gearbox,” Journal of Sound and Vibration, Vol. 144, pp. 163–172, 1991.
 9. Howard, I.M., “An investigation of Vibration Signal Averaging of Individual Components in an Epicyclic Gearbox,” Technical Report ARL–PROP–R–185, Australian Department of Defense, Aeronautical Research Laboratory, Mar. 1991.
 10. McFadden, P. D., “Window Functions for the Calculation of the Time Domain Averages of the Vibration of the Individual Planet Gears and Sun Gear in an Epicyclic Gearbox,” Journal of Vibration and Acoustics, Vol. 116, pp. 179–187, Apr. 1994.
 11. Forrester, D., “A Method for the Separation of Epicyclic Planet Gear Vibration Signatures,” Proceedings of Acoustical and Vibratory Surveillance Methods and Diagnostic Techniques, Senlis, France, pp. 539–548, Oct. 1998.
 12. Samuel, P.D., Conroy, J.K., and Pines, D.J., “Planetary Transmission Diagnostics,” NASA/CR—2004-213068, University of Maryland, NAG3–2223, May 2004.
 13. Mark, W.D., and Hines, J.A., “Stationary Transducer Response to Planetary-Gear Vibration Excitation with Non-Uniform Planet Loading,” Mechanical Systems and Signal Processing, Vol. 23, No. 4, pp. 1381.
 14. Mark, W.D., “Stationary Transducer Response to Planetary-Gear Vibration Excitation II: Effects of Torque Modulations,” Mechanical Systems and Signal Processing, Vol. 23, No. 7, pp. 2259.
 15. Bartelmus, W., and Zimroz, R., “Vibration Condition Monitoring of Planetary Gearbox under Varying External Load,” Mechanical Systems and Signal Processing, Vol. 23, No. 1, pp. 257.
 16. Lewicki, D.G., and Ballarini, R., “Effect of Rim Thickness on Gear Crack Propagation Path,” ASME Journal of Mechanical Design, Vol. 119, No. 1, Mar. 1997, pp. 88–95.
 17. Lewicki, D.G., Decker, H.J., and Shimski, J.T., “Development of a Full-Scale Transmission Testing Procedure to Evaluate Advanced Lubricants,” NASA TP–3265, AVSCOM TR–91–C–026, Aug. 1992.
 18. Howard, I., “A Review of Rolling Element Bearing Vibration: Detection, Diagnosis and Prognosis,” Aeronautical and Maritime Research Laboratory, Melbourne, Australia, DSTO–RR–0013, 1994.
 19. Samuel, P.D., and Pines, D.J., “A Review of Vibration-based Techniques for Helicopter Transmission Diagnostics,” Journal of Sound and Vibration, Vol. 282, No. 1–2, pp. 475–508, Apr. 2005.
 20. Martin, H.R., “Statistical Moment Analysis as a Means of Surface Damage Detection,” Proceedings of the Seventh International Modal Analysis Conference, Society for Experimental Mechanics, Schenectady, NY, 1989, pp. 1016–1021.

REPORT DOCUMENTATION PAGE			Form Approved OMB No. 0704-0188		
<p>The public reporting burden for this collection of information is estimated to average 1 hour per response, including the time for reviewing instructions, searching existing data sources, gathering and maintaining the data needed, and completing and reviewing the collection of information. Send comments regarding this burden estimate or any other aspect of this collection of information, including suggestions for reducing this burden, to Department of Defense, Washington Headquarters Services, Directorate for Information Operations and Reports (0704-0188), 1215 Jefferson Davis Highway, Suite 1204, Arlington, VA 22202-4302. Respondents should be aware that notwithstanding any other provision of law, no person shall be subject to any penalty for failing to comply with a collection of information if it does not display a currently valid OMB control number.</p> <p>PLEASE DO NOT RETURN YOUR FORM TO THE ABOVE ADDRESS.</p>					
1. REPORT DATE (DD-MM-YYYY) 01-11-2011		2. REPORT TYPE Technical Memorandum		3. DATES COVERED (From - To)	
4. TITLE AND SUBTITLE Planetary Gearbox Fault Detection Using Vibration Separation Techniques			5a. CONTRACT NUMBER		
			5b. GRANT NUMBER		
			5c. PROGRAM ELEMENT NUMBER		
6. AUTHOR(S) Lewicki, David, G.; LaBerge, Kelsen, E.; Ehinger, Ryan, T.; Fetty, Jason			5d. PROJECT NUMBER		
			5e. TASK NUMBER		
			5f. WORK UNIT NUMBER WBS 877868.02.07.03.01.01.01		
7. PERFORMING ORGANIZATION NAME(S) AND ADDRESS(ES) National Aeronautics and Space Administration John H. Glenn Research Center at Lewis Field Cleveland, Ohio 44135-3191			8. PERFORMING ORGANIZATION REPORT NUMBER E-17816		
9. SPONSORING/MONITORING AGENCY NAME(S) AND ADDRESS(ES) National Aeronautics and Space Administration Washington, DC 20546-0001			10. SPONSORING/MONITOR'S ACRONYM(S) NASA		
			11. SPONSORING/MONITORING REPORT NUMBER NASA/TM-2011-217127		
12. DISTRIBUTION/AVAILABILITY STATEMENT Unclassified-Unlimited Subject Category: 37 Available electronically at http://www.sti.nasa.gov This publication is available from the NASA Center for AeroSpace Information, 443-757-5802					
13. SUPPLEMENTARY NOTES					
14. ABSTRACT Studies were performed to demonstrate the capability to detect planetary gear and bearing faults in helicopter main-rotor transmissions. The work supported the Operations Support and Sustainment (OSST) program with the U.S. Army Aviation Applied Technology Directorate (AATD) and Bell Helicopter Textron. Vibration data from the OH-58C planetary system were collected on a healthy transmission as well as with various seeded-fault components. Planetary fault detection algorithms were used with the collected data to evaluate fault detection effectiveness. Planet gear tooth cracks and spalls were detectable using the vibration separation techniques. Sun gear tooth cracks were not discernibly detectable from the vibration separation process. Sun gear tooth spall defects were detectable. Ring gear tooth cracks were only clearly detectable by accelerometers located near the crack location or directly across from the crack. Enveloping provided an effective method for planet bearing inner- and outer-race spalling fault detection.					
15. SUBJECT TERMS Gear teeth; Cracks; Transmissions (machine elements); Defects; Vibration					
16. SECURITY CLASSIFICATION OF:			17. LIMITATION OF ABSTRACT UU	18. NUMBER OF PAGES 21	19a. NAME OF RESPONSIBLE PERSON STI Help Desk (email:help@sti.nasa.gov)
a. REPORT U	b. ABSTRACT U	c. THIS PAGE U			19b. TELEPHONE NUMBER (include area code) 443-757-5802

